Article

Mechanical Response of Polymer Epoxy/BMI Composites with Graphene and a Boron Nitride Monolayer from First Principles

Geeta Sachdeva,* Álvaro Lobato, Ravindra Pandey,* and Gregory M. Odegard

Cite This: https://dx.doi.org/10.1021/acsapm.0c01306

Read Online

ACCESS | 📊 Metrics & More | 📱 Article Recommendations | 🆁 Supporting Information

ABSTRACT: Polymer composites possess an integrated combination of structures and properties associated with the host matrix and the fiber material and thus hold the potential of being high-strength materials. In general, the load transfer from the matrix to the fiber depends upon the strength of bonding at the interface, which characterizes the mechanical strength. In this work, first-principles calculations based on the density functional theory are employed to provide the molecular-level description of the interface formed by resins (i.e., diglycidyl ether of bisphenol A (DGEBA) and 4′-bismaleimidodiphenylmethane (BMPM)) or hardeners (i.e., diethyl toluene diamine (DETDA) and o,o′-diallyl bisphenol A (DABPA)) with graphene (or boron nitride (BN) monolayer). The results show that the interaction strength between a resin (or hardener) and graphene is mainly governed by the nature of bonding at the interface, and subsequently, the mechanical response follows the hierarchical order of the interaction strength at the interface; the transverse stiffness of BMPM/graphene is higher than that of DGEBA/graphene. Moreover, the change in the polarity of the surface from graphene to the BN monolayer improves the superior interfacial strength and thereby a higher transverse stiffness of both resin and hardener composites at the molecular level. These results emphasize the need to use computational modeling to efficiently and accurately determine molecular-level polymer/surface combinations that yield optimal mechanical performance of composite materials. This is especially important in the design and development of high-performance composites with nanoscale reinforcement.

KEYWORDS: mechanical properties, epoxy, BMI, graphene, BN monolayer, density functional theory
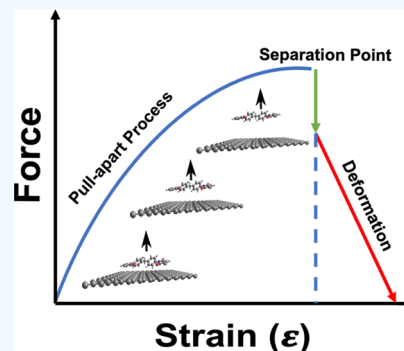
1. INTRODUCTION

In a fiber−polymer composite system, fibers play an important role of load-bearing components, and the polymer matrix provides support to fibers by maintaining their orientations in the composite. In recent years, the use of carbon nanotubes (CNT) as a fiber element has helped to make significant advances in transport technology due to their low weight-to-stiffness ratio, resistance to environmental impact, and processability.[1−3] The C−C covalent bond in carbon rings, which is regarded as the most stable chemical bond in nature, endows graphitic surfaces with excellent mechanical properties,[4,5] thereby making them promising candidates for the next generation of high-performance composites. For example, Young's modulus of CNTs with a density of 1.33 g/cm³ can be as high as 1 TPa.[6−8] Therefore, focused scientific efforts have been invested in engineering CNT-based composites that exploit the outstanding mechanical properties of individual CNTs. However, the stiffness and strength of individual CNTs have generally not transferred well to large-scale assemblages.

To address the abovementioned challenge, both experimental[9−12] and theoretical[13−16] methods have been used to investigate the interface formed by a CNT fiber with the polymer matrix to gain insight into its role in determining the mechanical response of the composite. For example, it has been shown that sliding occurs within the fractured fibers of long CNTs leading to a poor load transfer,[17] and multiwalled CNTs are often deformed and twisted, which increases their flexibility.[18] One weakness of CNT assemblages is the inadequate noncovalent interaction between adjacent circular CNTs, which leads to the slippage of CNTs during deformation.[17] Hence, it was recently proposed to fabricate self-assembled stacks of large-diameter (∼10 nm) CNTs, referred to as flattened CNTs (flCNTs), which maximizes the contact area between CNTs, and thus the noncovalent type of bonding.[19] Therefore, it appears possible that the mechanical properties of the flCNT composite may be further enhanced by carefully engineering its interface.

Also, flattened CNTs, which are referred to as a "dog-bone"-type collapse in the scientific literature, have been linked to improved mechanical performance because of their similarity to graphitic carbon.[20] They can be considered as stacked layers
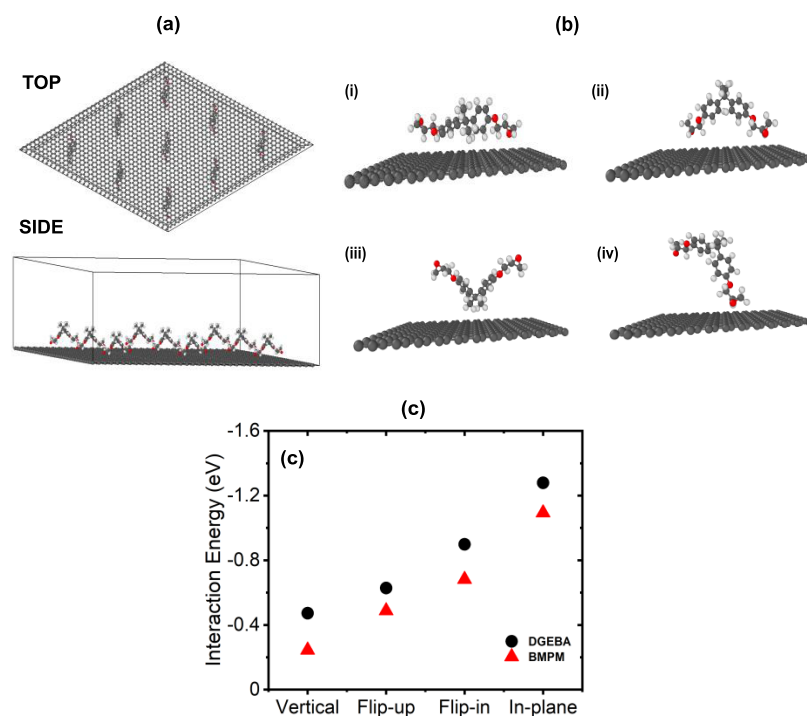
Figure 1. (a) Top and side views of a complex. (b) Molecular orientations: (i) in-plane, (ii) flip-in, (iii) flip-up, and (iv) vertical over graphene. Atomic color codes—O (red), C (gray), and H (white). (c) Orientation-dependent interaction energy of DGEBA (red) and BMPM (black) interacting with graphene.

of graphene, which is a two-dimensional hexagonal monolayer with sp^2 hybridized covalent bonds.[21] The van der Waals (vdW) interaction terms between the graphene planes provide the stability to flattened CNTs that possess reactive edges, and the curvature of which can be used to control not just chemical and mechanical properties, but thermal and electronic properties as well.[22]

Among polymers, epoxies containing epoxide groups and bis-maleimides (BMI) containing maleimide groups (Figure S1) are the most commonly used thermosetting resins[23] for making high-performance composites because they provide a unique balance of thermal and mechanical properties combined with extreme processing versatility.[24,25] It is worth mentioning that diglycidyl ether of bisphenol A (DGEBA) and 4′-bismaleimidodiphenylmethane (BMPM) are some of the most widely used high-performance epoxies and BMI resins in the aerospace industry. For example, the fifth-generation combat aircraft F-35 Lightning II developed by Lockheed Martin is stated to consist of about 35% carbon fiber composites out of the entire structural weight, and the primary structural composites used in the aircraft are composed of either epoxy or BMI matrices. Although other matrices like polyethylene and polystyrene facilitate a mechanical response at room temperature that satisfies property requirements for some applications, there exist challenges in using such matrices in more rigorous applications as it does not perform well at elevated temperatures.[26,27] This is not the case with either epoxy (DGEBA) or BMI (BMPM) as both are stable at elevated temperatures.[28,29] Note that DGEBA and BMPM monomers are often crosslinked with diethyl toluene diamine (DETDA) and *o,o′*-diallyl bisphenol A (DABPA) monomers, respectively. DETDA is an aromatic amine curing agent, and DABPA is allylphenol that offers excellent toughness to the BMPM.[30,31]

In general, a detailed understanding of the interaction between graphene and a resin (hardener) matrix at the molecular level is crucial for improving the composite's mechanical response. This is because the adhesion between a resin (hardener) and graphene is related to the chemistry of the interface[2,32] which has, without any doubt, a considerable influence on the fracture/failure behavior of a composite, although it is not yet understood completely. We are aware of only a few theoretical studies based on atomistic modeling that were used to characterize the interfacial bonding in composites.[33−35] Overall, it has been recognized that the interface plays a significant role in the stress transfer and the consequent improvements in the composite stiffness and strength.[36,37]

In the following, we will present the results related to graphene/resins (hardeners) focusing on the characterization of the interface at the molecular level using a periodical supercell model. The mechanical response in terms of the separation point (or breaking point) and stiffness will be determined. Within this atomic framework, one can directly modify the interface, even with modifications that are extremely difficult or impossible to control in the experiment, to predict the consequences on the interfacial strength and thereby its mechanical response.

The resin (hardener) monomers, DGEBA (DETDA) and BMPM (DABPA), interacting with the surface of graphene are explored. Figure 1a shows the top and side views of a monomer forming a complex with graphene in a periodic supercell. It should be noted that our focus is not on the cured polymer composites, rather on individual monomers to provide a fundamental understanding of the structure−property relationship in graphene−polymer composites. Moreover, we will also consider the cases of these monomers interacting with a boron nitride (BN) monolayer to benchmark

the results obtained for monomer/graphene complexes. Both graphene and BN monolayer are structurally similar, but electronically dissimilar materials; the covalently linked graphene is a zero-gap material, whereas the semi-ionic h-BN monolayer, which has a nearly identical honeycomb config-uration as that of graphene, is semiconducting.[38]

2. COMPUTATIONAL METHOD

Electronic structure calculations were performed using projector-augmented wave (PAW) potentials within the framework of the density functional theory (DFT), as implemented in the Vienna ab initio simulation package (VASP).[39] The exchange and correlation potentials were treated using a generalized gradient approximation (GGA) with the Perdew−Burke−Ernzerhof (PBE) functional form.[40] Contributions from the van der Waals (vdW) interactions, which are important for graphitic systems, were incorporated using Grimme's semiempirical dispersive D2 term.[41] The energy cut-off and the convergence criterion of the energy were 500 and 10^{-5} eV, respectively.

In a supercell, the periodic boundary conditions with a lateral separation along the c-direction of 20 Å were employed to ensure the negligible interaction between the periodic images. The relaxation process for the equilibrium config-uration was carried out by placing a monomer on the top of graphene in various orientations, and the distances between them were set to a value that was slightly larger (or similar to) than the sum of the nearest resin (hardener) atom and covalent radii of carbon atoms. The structure was then relaxed using the conjugate gradient algorithm until the maximum forces acting on the atoms became smaller than 0.001 eV/Å.

The mechanical response of the complex consisting of a resin (or hardener) and graphene (or BN monolayer) was investigated in a way that mimics the "pull-apart" experimental setup commonly used for polymer composites.[9,42−44] In our setup, a resin, which was in the equilibrium configuration, was pulled up along the direction perpendicular to the surface of the constrained (frozen) graphene. DFT calculations were performed for each step of the pull-apart process to generate the energy surface describing the interaction of a resin (hardener) with graphene.

In the pull-apart setup, we define the tensile strain to be the perpendicular displacement between a resin (hardener) and the surface of the monolayer with respect to the equilibrium separation. In this way, the strain ε can then be defined as $\varepsilon = (l - l_0) l_0$, where l is the displacement of the resin (hardener) with respect to the distance l_0 calculated in the equilibrium configuration of the complex. The mechanical properties can then be calculated from the strain−energy relationship, $E_s = E(\varepsilon) - E(0)$; the energy difference between systems under a given strain ε and no strain is associated with the equilibrium configuration.

The calculated strain−energy curve is used to obtain the force vs strain curve, which can be used in the spinodal equation of state[45] to determine the critical force and critical strain of a given complex. It is worth mentioning that the spinodal equation of state, in general, applies to the bulk material, but its use has been extended to low-dimensional materials, including graphene and the BN monolayer.

It has been shown that the one-dimensional (1D) spinodal equation of state can reproduce stress dependence on the strain energy of a given system.[45−47] The equation of state can be written as

$$\sigma = \sigma_{sp}\left(1 - \left(\frac{\epsilon_{sp} - \epsilon}{\epsilon_{sp}}\right)^{1/1-\gamma}\right) \tag{1}$$

where ϵ and ϵ_{sp} represent the strain at a particular point and the spinodal strain, respectively. γ is a pseudocritical exponent that varies with the direction of (stretching or compressing) strain. Equation 1 can be written in terms of the force by multiplying the stress terms with the effective area as follows

$$f = f_{sp}\left(1 - \left(\frac{\epsilon_{sp} - \epsilon}{\epsilon_{sp}}\right)^{1/1-\gamma}\right) \tag{2}$$

An interesting feature of the proposed force−strain equation of state is that it can also be expressed analytically in its energy form. Considering the isotherm at 0 K, the force is related to the internal energy E and the equilibrium length L employing the relationship of $f = \frac{1}{L}\frac{dE}{d\epsilon}$. Here, f_{sp} accounts for the maximum force at which the system breaks and therefore represents the elastic limit of the material. It is referred to as the critical force. The value of the strain corresponding to the critical force is called the critical strain. In the following discussion, we designate the critical strength to represent (out-of-plane) the transverse strength and the critical strain to be (out-of-plane) the separation point at which the monomer breaks from the monolayer. E can be understood as the energy needed for the out-of-plane pull-apart (or separation) of the resin (hardener) from the surface and, therefore, to overcome the interatomic forces binding the complex.

3. RESULTS AND DISCUSSION

3.1. Interaction Energy. Initial DFT calculations were performed to determine the equilibrium configurations of resin (DGEBA and BMPM) and hardener (DETDA and DABPA) molecules. Figure S2 displays the structural configurations of these molecules, and Table S1 lists the calculated C−C and B−N bond lengths (∼1.42 Å), which were in excellent agreement with previous reports.[38,48,49]

In calculations of the energy surface describing the interaction of a resin (hardener) with the monolayer, we allowed it to approach the surface in the direction perpendicular to the surface with a specific orientation while keeping the monolayer fixed. For example, DGEBA is oriented in such a way that (i) both end groups and hydrogen ends are oriented toward the surface—the in-plane orientation (Figure 1b(i)), (ii) both the epoxide end groups are facing the surface, and the hydrogen end is away from the surface—the flip-in orientation (Figure 1b(ii)), (iii) both the end epoxide groups are aligned away from the surface, and the hydrogen end is close to the surface—the flip-up orientation (Figure 1b(iii)), and (iv) only one end group is facing the surface—the vertical orientation (Figure 1b(iv)). At the minimum energy distance associated with a specific orientation, full optimization of the conjugated system in which all atoms were free to relax was performed.

The characteristics of the complexes are determined in terms of the interaction energy, the area of contact, the population of atoms, Bader's charge,[50] critical force, and critical strain. We define the interaction energy (ΔE) as E (complex) − E (resin (hardener)) − E (monolayer), and a negative value of ΔE suggests the stability of the complex. ΔE can also be

considered as the adsorption energy of a resin (hardener) on the monolayer. The contact area is the area of the resin (hardener) projected on the surface of the monolayer. The population of atoms is defined as the number of the resin (hardener) atoms within the range 3 Å from the surface. Note that the interplanar distance of ~3 Å can be taken as the characteristic distance of vdW-bound systems including the complexes considered.[51]

Figure 1c shows the calculated values of the interaction energies of DGEBA and BMPM forming a complex with graphene. The results show the in-plane orientation to be energetically preferred, and it is followed by flip-in, flip-up, and vertical orientations. The interaction energy steadily increases by ~0.9 eV in going from vertical to in-plane orientations, thereby suggesting that graphene prefers the resin to be aligned parallel to the surface. Table S2 lists the interaction energy, the bond distances at the interface, the area of contact, and population of atoms of the equilibrium configurations of the abovementioned cases.

Next, we calculate the effective area of contact using the estimated length and width of the surface covered by a resin (hardener) using its distance of one end to the other in both x- and y-directions. We find that the calculated area for the "in-plane" orientation is significantly higher than those of the rest of the orientations for both cases (Table S2). This is further corroborated by calculations of the population of atoms by counting the number of atoms that are within the range of ~3 Å above the surface. The results show that the in-plane population is significantly larger than those of the other three orientations, thereby facilitating a larger degree of interaction between the resin atoms and graphene at the interface. Subsequently, the in-plane orientation leads to the energetically preferred configuration for DGEBA and BMPM on graphene. We note that our results are in line with the PBE (DFT) results on the DGEBA/CNT complex, reporting the preference of the longitudinal orientation over the transverse orientation of DGEBA on a CNT.[52]

Both resins and hardeners consist of aromatic rings and side groups containing oxygen or nitrogen atoms. However, graphene consists of a honeycomb lattice, in which C atoms form in-plane sp^2 hybridized bonds together with out-of-plane π-bonds. The interaction of a resin (or hardener) with graphene is, therefore, expected to be governed by $\pi-\pi$ noncovalent interactions with a small contribution from the polarizable O and N atoms of the side groups. This is what has been affirmed by the analysis of the interface in terms of the area of contact and the population of atoms; a large effective contact area and population of atoms yield the in-plane orientation to be the energetically preferred configuration of a resin (hardener) on graphene.

Figure S3 displays the (in-plane) equilibrium configurations of the complexes, and the calculated values of the corresponding interaction energy values are listed in Table 1. For the complexes, the calculated results show that the order of the interaction strength is DGEBA < BMPM for resins and DETDA < DABPA for hardeners. Specifically, the difference between the interaction strengths of DGEBA and BMPM is noticeable and can be explained in terms of the population of atoms, which is significantly larger for DGEBA (Table 1). Furthermore, the polarizable O atoms (of DGEBA) induce a hybridized state that appears in the valance band region of the density of states, though the H (resin)−C (graphene)

Table 1. Interaction Energy (ΔE), the Population of Atoms, and Bader's Charge (Q) Calculated for Resin and Hardener Complexes

|	complex (in-plane)	ΔE (eV)	population of atoms (%)	$Q_{graphene}$ (e)
resin	DGEBA/graphene	−1.27	16	0.03
	BMPM/graphene	−1.09	10	0.05
	DGEBA/BN	−1.33	16	0.03
	BMPM/BN	−1.30	15	0.06
hardener	DETDA/graphene	−0.96	20	0.04
	DABPA/graphene	−0.74	11	0.02
	DETDA/BN	−1.24	20	0.02
	DABPA/BN	−0.86	11	0.02

hybridized states dominate the valence band in both resin complexes (Figure 2c,d).

For the case of the BN monolayer, we expect a small but noticeable difference in the calculated results as compared to those obtained for graphene. This is because the BN monolayer being semi-ionic may induce a slightly higher degree of electrostatic interaction with a resin (hardener) relative to graphene. The calculated values of the interaction energy are higher; $DGEBA_{(graphene)} < DGEBA_{(BN)}$ and $BMPM_{(graphene)} < BMPM_{(BN)}$ for the resin complexes and $DABPA_{(graphene)} < DABPA_{(BN)}$ and $DETDA_{(graphene)} < DETDA_{(BN)}$ for the hardener complexes.

Moreover, the results indicate that curing agents (e.g., DETDA) participate effectively at the interface, which implies that the load transfer of epoxy/graphene composites is governed by both the resin and the hardener in this case. The interaction energy values for DETDA and DABPA are in line with the expectations arising from their values of the population of atoms (Table 1). It is worth mentioning that the aromatic ring of DETDA is aligned parallel to graphene and thereby yielding a higher degree of the vdW interaction with monolayers at the interface.

Overall, the interaction between the resin (or hardener) and graphene (or BN monolayer) is governed by the dispersive force like vdW in the cases considered. This is due to the fact that the analysis of the calculated Bader charge suggests the occurrence of a small charge transfer (<0.1 e) from graphene (BN monolayer) to resins (hardeners) (Table 1). Moreover, the hydrogen-bonding interactions with π electrons of graphene (or B/N atoms of BN monolayer) at the separation of 2.5 Å are expected to be weak.[53]

3.2. Mechanical Response. The (out-of-plane) mechanical response of the complexes was calculated using the setup and by applying the load in only the "z"-direction, which is perpendicular to the surface starting from its equilibrium separation to the separation of ≈3.8 Å with a step-size of 0.02 Å (Figure S4). DFT calculations were performed at each step generating the energy surface of the resin (DGEBA or BMPM) and the hardener (DABPA or DETDA) forming complexes with graphene (or BN monolayer) (Figure S5). The strain (or separation)-energy surfaces were then used to calculate force vs strain curves, as shown in Figure 3. Subsequently, the force vs strain curve was used in the 1D spinodal equation of state (eq 2). We noted that two parameters, f_c and ε_c, defined the shape of each curve, which was used to characterize the
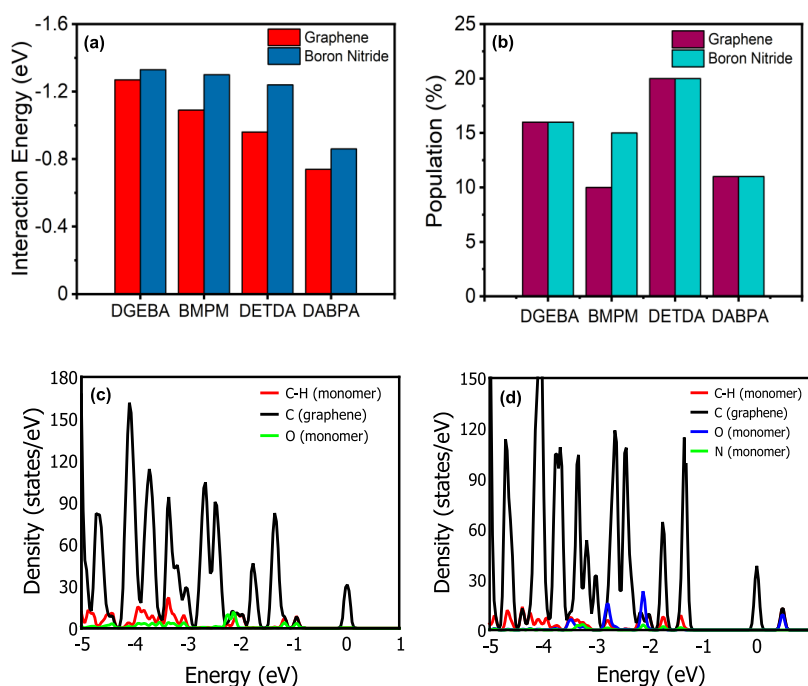
Figure 2. (a) Calculated interaction energy of resins (DGEBA and BMPM) and hardeners (DABPA and DETDA) with graphene (red) and the BN monolayer (blue). (b) Calculated population of atoms within the range of 3 Å distance above the monolayer. Atom-projected density of states for (c) resin DGEBA with graphene and (d) resin BMPM with graphene.
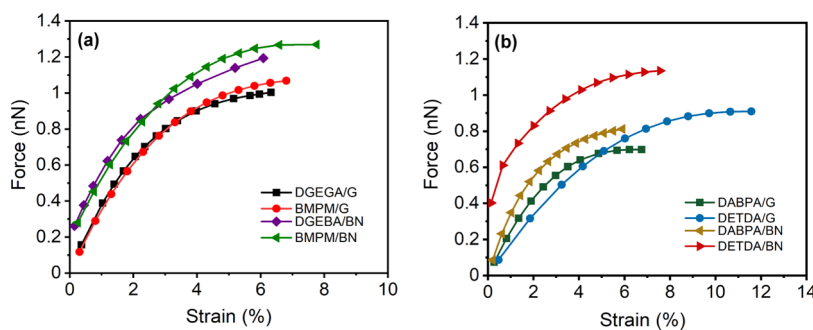
Figure 3. Calculated force vs transverse strain curves of the (a) resin (DGEBA or BMPM) and (b) hardener (DABPA or DETDA) forming complexes with graphene (or BN monolayer).

transverse strength and the separation point of the conjugated monomers considered (Table 2). γ is the 1D correspondence of the pseudocritical exponent β, which, in general, takes a value of 0.85 associated with the volumetric compression of

Table 2. Calculated Values of the Transverse Strength and (Out-of-Plane) the Separation Point of the Complexes

	complex	transverse strength f_c (nN)	(out-of-plane) separation point ε_c (%)
resin	DGEBA/ graphene	1.0	6.3
	BMPM/ graphene	1.1	6.8
	DGEBA/BN	1.2	6.1
	BMPM/BN	1.3	7.7
hardener	DETDA/ graphene	0.9	11.6
	DABPA/ graphene	0.7	6.7
	DETDA/BN	1.1	7.6
	DABPA/BN	0.8	5.9

solids.[54,55] In the case presented, γ varies between 0.5 and 0.8 (Table S3).

It is worth mentioning that the equation of state (e.g., eq 1), in general, is used to investigate the constitutive responses of a bulk-like system. In the case presented, we have used the spinodal equation of state to differentiate the (out-of-plane) mechanical response of quasi-three-dimensional (3D) complexes consisting of a resin (hardener) and graphene (BN monolayer). Therefore, in the following discussion, we use "transverse" to describe the out-of-the-plane and designate the critical strength to represent the transverse strength and the critical strain to be (out-of-plane) the separation point at which the monomer apart from the monolayer (Figure S6).

The calculated results show that the resin (hardener) forming complexes with the BN monolayer exhibit a slightly higher transverse strength than the corresponding complexes with graphene. Among resins, BMPM exhibits a slightly higher transverse strength relative to that of DGEBA. This is not the case with the separation point values for which we find the order to be DGEBA/graphene $\approx$ DGEBA/BN < BMPM/ graphene < BMPM/BN. Interestingly, the hardener DETDA
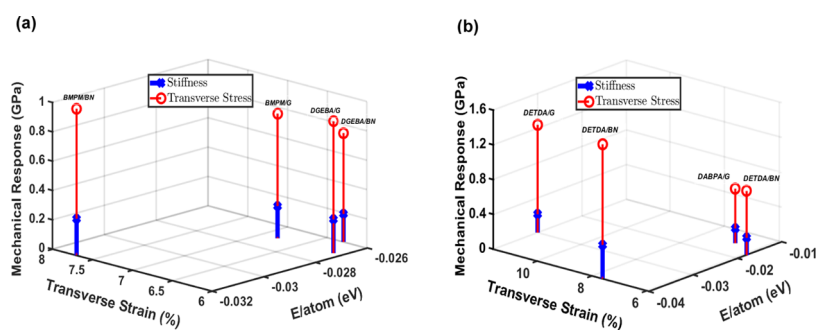
Figure 4. Interaction energy/atom vs transverse strain and stiffness for the (a) resin (DGEBA or BMPM) and (b) hardener (DABPA or DETDA) forming complexes with graphene (or BN monolayer).

exhibits a relatively high value of the separation point suggesting that, as a curing agent, it is likely to improve the interfacial load transfer of the epoxy/graphene composite. It is worth noting that the calculated transverse strength of DGEBA/graphene is comparable to the calculated value of DGEBA/CNT; MD calculations reported the value of the force to be ∼3.8 nN, which breaks a DGEBA strand from a CNT,[29] whereas we find the value of ∼1 nN to break the DGEBA from graphene (Table 2).

In general, the (out-of-plane) stiffness can be taken as a measure of the quasi-3D Young's modulus suggesting that a higher value of the stiffness leads to a higher Young's modulus, which is one of the desired characteristics of an engineered composite.

Table S4 lists the values of the transverse stress and stiffness calculated from the stress−strain curve displayed in Figure S7 for which the area is estimated by projecting the length and width of the resin (hardener) over graphene (or BN monolayer). The results show that BMPM/graphene (or BMPM/BN) is stiffer than the corresponding DGEBA complexes. Among the hardeners considered, DETDA having a (graphene-like) planar structure is predicted to have higher stiffness than DABPA in the complexes considered. Next, we benchmark our stiffness values to the values calculated for bilayer graphene employing a similar pull-apart setup. The elastic stiffness of bilayer graphene is calculated to be 24 GPa, an order of magnitude higher than what is predicted for the resin (or hardener) forming complexes with graphene. This is in line with the expectation of the occurrence of a relatively high degree of vdW interactions at the interface with a 100% population of atoms for the case of bilayer graphene.

Finally, Figure 4 summarizes the result of the present study displaying the predicted relationship between the interaction strength at the interface and the mechanical response in terms of stiffness obtained at the molecular level for epoxy and BMI composites. The results show that the mechanical response is directly related to the degree of the interface adhesion, though it can also be influenced by the nature of the chemical bonds at the interface in the polymer composites.

4. SUMMARY

We performed an atomistic investigation of the representative polymer composites employing the density functional theory to establish the relationship between the nature of the interface and its mechanical response. Specifically, DGEBA (DETDA) and BMPM (DABPA) were considered to represent resin (hardener) components of the epoxy and BMI, respectively. The calculated results indicated that the interfacial adhesion was highly influenced by the orientation of the resin (hardener) on graphene due to van der Waals interactions being dominated at the interface. Next, we used the strain−energy relationship to extract force vs strain curves, which were then used in the 1D spinodal equation of state to determine the mechanical response of a complex. We found that the mechanical response in terms of stiffness follows the hierarchical order of the interaction strength at the interface; elastic stiffness of BMPM/graphene was higher than that of DGEBA/graphene. The change in polarity of the surface from graphene to the BN monolayer improved the interfacial strength and thereby the elastic stiffness due to the presence of covalent polar bonds at the interface. Furthermore, the presence of aromatic rings in the hardener DETDA yielded a significantly higher mechanical response relative to the one exhibited by the DABPA hardener suggesting that DETDA, as a curing agent, was likely to improve the interfacial load transfer of the epoxy/graphene composite. Overall, the results predicted that a small degree of polarity at the interface dominated by van der Waals interactions can help in improving its mechanical response. In light of the intricate molecular-level simulations based on first-principles methods, predicting the interfacial properties of composites is challenging but can provide an insight to experimentalists in tailoring composites properties as demanded by aerospace applications.

■ ASSOCIATED CONTENT

*ⓢ Supporting Information

The Supporting Information is available free of charge at https://pubs.acs.org/doi/10.1021/acsapm.0c01306.

> Epoxide and maleimide groups; structural configurations and geometrical parameters of resin and hardener monomers; orientation-dependent properties of complexes; pull-apart force mechanism; mechanical response of the complexes simulated in a periodic supercell (PDF)

■ AUTHOR INFORMATION

Corresponding Authors

Geeta Sachdeva − *Department of Physics, Michigan Technological University, Houghton, Michigan 49931, United States*; Email: gsachdev@mtu.edu

Ravindra Pandey − *Department of Physics, Michigan Technological University, Houghton, Michigan 49931, United States*; ⓞ orcid.org/0000-0002-2126-1985; Email: pandey@mtu.edu

Authors

Álvaro Lobato − *MALTA-Consolider Team and Departamento de Química Física y Analítica, Universidad de Oviedo, E-33006 Oviedo, Spain*

Gregory M. Odegard − *Department of Mechanical Engineering and Engineering Mechanics, Michigan Technological University, Houghton, Michigan 49931, United States;* ⊙ orcid.org/0000-0001-7577-6565

Complete contact information is available at:
https://pubs.acs.org/10.1021/acsapm.0c01306

Notes

The authors declare no competing financial interest.

■ REFERENCES

(1) Radue, M. *Molecular Modeling of Aerospace Polymer Matrices Including Carbon Nanotube-Enhanced Epoxy*, 2017.

(2) Melro, L.; Pyrz, R.; Jensen, L. R. In *A Molecular Dynamics Study on the Interaction Between Epoxy and Functionalized Graphene Sheets*. 37th Risø International Symposium on Materials Science; IOP Publishing, 2016; pp 363−372.

(3) Iijima, S. Helical microtubules of graphitic carbon. *Nature* **1991**, *354*, 56−58.

(4) Iijima, S.; Brabec, C.; Maiti, A.; Bernholc, J. Structural flexibility of carbon nanotubes. *J. Chem. Phys.* **1996**, *104*, 2089−2092.

(5) Cornwell, C.; Wille, L. Elastic properties of single-walled carbon nanotubes in compression. *Solid State Commun.* **1997**, *101*, 555−558.

(6) Popov, V. N. Carbon nanotubes: properties and application. *Mater. Sci. Eng., R* **2004**, *43*, 61−102.

(7) Thostenson, E. T.; Li, C.; Chou, T.-W. Nanocomposites in context. *Compos. Sci. Technol.* **2005**, *65*, 491−516.

(8) Treacy, M. M. J.; Ebbesen, T. W.; Gibson, J. M. Exceptionally high Young's modulus observed for individual carbon nanotubes. *Nature* **1996**, *381*, 678−680.

(9) Chandra, Y.; Scarpa, F.; Adhikari, S.; Zhang, J.; Flores, E. S.; Peng, H.-X. Pullout strength of graphene, and carbon nanotube/epoxy composites. *Composites, Part B* **2016**, *102*, 1−8.

(10) Xiong, Q.; Meguid, S. Atomistic investigation of the interfacial mechanical characteristics of carbon nanotube reinforced epoxy composite. *Eur. Polym. J.* **2015**, *69*, 1−15.

(11) Manoharan, M.; Sharma, A.; Desai, A.; Haque, M. A.; Bakis, C. E.; Wang, K. The interfacial strength of carbon nanofiber epoxy composite using single fiber pullout experiments. *Nanotechnology* **2009**, *20*, No. 295701.

(12) Ganesan, Y.; Peng, C.; Lu, Y.; Loya, P. E.; Moloney, P.; Barrera, E.; Yakobson, B. I.; Tour, J. M.; Ballarini, R.; Lou, J. Interface toughness of carbon nanotube reinforced epoxy composites. *ACS Appl. Mater. Interfaces* **2011**, *3*, 129−134.

(13) Li, Y.; Seidel, G. Multiscale modeling of the interface effects in CNT-epoxy nanocomposites. *Comput. Mater. Sci.* **2018**, *153*, 363−381.

(14) Zhang, Y.; Zhuang, X.; Muthu, J.; Mabrouki, T.; Fontaine, M.; Gong, Y.; Rabczuk, T. Load transfer of graphene/carbon nanotube/polyethylene hybrid nanocomposite by molecular dynamics simulation. *Composites, Part B* **2014**, *63*, 27−33.

(15) Radue, M.; Odegard, G. M. Multiscale modeling of carbon fiber/carbon nanotube/epoxy hybrid composites: Comparison of epoxy matrices. *Compos. Sci. Technol.* **2018**, *166*, 20−26.

(16) Odegard, G. M.; Gates, T.; Wise, K.; Park, C.; Siochi, E. Constitutive modeling of nanotube-reinforced polymer composites. *Compos. Sci. Technol.* **2003**, *63*, 1671−1687.

(17) Zhang, X.; Li, Q.; Holesinger, T. G.; Arendt, P. N.; Huang, J.; Kirven, P. D.; Clapp, T. G.; DePaula, R. F.; Liao, X.; Zhao, Y.; et al. Ultrastrong, stiff, and lightweight carbon-nanotube fibers. *Adv. Mater.* **2007**, *19*, 4198−4201.

(18) Yu, M.-F.; Kowalewski, T.; Ruoff, R. S. Structural analysis of collapsed, and twisted and collapsed, multiwalled carbon nanotubes by atomic force microscopy. *Phys. Rev. Lett.* **2001**, *86*, No. 87.

(19) Downes, R. D.; Hao, A.; Park, J. G.; Su, Y.-F.; Liang, R.; Jensen, B. D.; Siochi, E. J.; Wise, K. E. Geometrically constrained self-assembly and crystal packing of flattened and aligned carbon nanotubes. *Carbon* **2015**, *93*, 953−966.

(20) Motta, M.; Moisala, A.; Kinloch, I. A.; Windle, A. H. High performance fibres from 'dog bone' carbon nanotubes. *Adv. Mater.* **2007**, *19*, 3721−3726.

(21) Papageorgiou, D. G.; Kinloch, I. A.; Young, R. J. Mechanical properties of graphene and graphene-based nanocomposites. *Prog. Mater. Sci.* **2017**, *90*, 75−127.

(22) Choi, D.; Wang, Q.; Azuma, Y.; Majima, Y.; Warner, J.; Miyata, Y.; Shinohara, H.; Kitaura, R. Fabrication, and characterization of fully flattened carbon nanotubes: a new graphene nanoribbon analogue. *Sci. Rep.* **2013**, *3*, No. 1617.

(23) Miracle, D. Metal matrix composites−from science to technological significance. *Compos. Sci. Technol.* **2005**, *65*, 2526−2540.

(24) Atif, R.; Inam, F. Influence of macro-topography on damage tolerance and fracture toughness of monolithic epoxy for tribological applications. *World J. Eng. Technol.* **2016**, *04*, 335.

(25) Morgan, R. J.; Shin, E. E.; Rosenberg, B.; Jurek, A. Characterization of the cure reactions of bismaleimide composite matrices. *Polymer* **1997**, *38*, 639−646.

(26) Biron, M. *Thermoplastics, and Thermoplastic Composites*; William Andrew, 2018.

(27) Agarwal, B. D.; Broutman, L. J.; Chandrashekhara, K. *Analysis, and Performance of Fiber Composites*; John Wiley & Sons, 2006.

(28) Eftekhari, M.; Fatemi, A. Tensile, creep and fatigue behaviors of short fibre reinforced polymer composites at elevated temperatures: a literature survey. *Fatigue Fract. Eng. Mater. Struct.* **2015**, *38*, 1395−1418.

(29) Aglan, H.; Qian, Z.; Mitra-Majumdar, D. The effect of temperature on the critical failure properties of advanced polymer composites. *Polym. Test.* **1992**, *11*, 169−184.

(30) Pilato, L. A.; Michno, M. J. *Advanced Composite Materials*; Springer Science & Business Media, 1994.

(31) Morgan, R. J.; Jurek, R. J.; Yen, A.; Donnellan, T. Toughening procedures, processing, and performance of bismaleimide-carbon fibre composites. *Polymer* **1993**, *34*, 835−842.

(32) Chahal, R.; Adnan, A.; Roy, A. In *Molecular Dynamics Study of Carbon Nanotube/Epoxy Interfaces Using ReaxFF*. Proceedings of the American Society for Composites—Thirty-Second Technical Conference, 2017.

(33) Li, Y.; Liu, Y.; Peng, X.; Yan, C.; Liu, S.; Hu, N. Pull-out simulations on interfacial properties of carbon nanotube-reinforced polymer nanocomposites. *Comput. Mater. Sci.* **2011**, *50*, 1854−1860.

(34) Stamboulis, A.; Baillie, C.; Schulz, E. Interfacial characterisation of flax fibre-thermoplastic polymer composites by the pull-out test. *Angew. Makromol. Chem.* **1999**, *272*, 117−120.

(35) Tsafack, T.; Alred, J. M.; Wise, K. E.; Jensen, B.; Siochi, E.; Yakobson, B. I. Exploring the interface between single-walled carbon nanotubes and epoxy resin. *Carbon* **2016**, *105*, 600−606.

(36) Han, Y.; Elliott, J. Molecular dynamics simulations of the elastic properties of polymer/carbon nanotube composites. *Comput. Mater. Sci.* **2007**, *39*, 315−323.

(37) Moniruzzaman, M.; Sahin, A.; Winey, K. I. Improved mechanical strength and electrical conductivity of organogels containing carbon nanotubes. *Carbon* **2009**, *47*, 645−650.

(38) Zhong, X.; Yap, Y. K.; Pandey, R.; Karna, S. P. First-principles study of strain-induced modulation of energy gaps of graphene/BN and BN bilayers. *Phys. Rev. B* **2011**, *83*, No. 193403.

(39) Kresse, G.; Joubert, D. From ultrasoft pseudopotentials to the projector augmented-wave method. *Phys. Rev. B* **1999**, *59*, No. 1758.

(40) Perdew, J. P.; Burke, K.; Ernzerhof, M. Generalized gradient approximation made simple. *Phys. Rev. Lett.* **1996**, *77*, No. 3865.

(41) Grimme, S. Semiempirical GGA-type density functional constructed with a long-range dispersion correction. *J. Comput. Chem.* **2006**, *27*, 1787−1799.

(42) Barber, A. H.; Cohen, S. R.; Wagner, H. D. Measurement of carbon nanotube-polymer interfacial strength. *Appl. Phys. Lett.* **2003**, *82*, 4140−4142.

(43) Cooper, C. A.; Cohen, S. R.; Barber, A. H.; Wagner, H. D. Detachment of nanotubes from a polymer matrix. *Appl. Phys. Lett.* **2002**, *81*, 3873−3875.

(44) DiFrancia, C.; Ward, T. C.; Claus, R. O. The single-fibre pull-out test. 1: Review and interpretation. *Composites, Part A* **1996**, *27*, 597−612.

(45) Chorfi, H.; Lobato, Á.; Boudjada, F.; Salvadó, M. A.; Franco, R.; Baonza, V. G.; Recio, J. M. Computational Modeling of Tensile Stress Effects on the Structure and Stability of Prototypical Covalent and Layered Materials. *Nanomaterials* **2019**, *9*, No. 1483.

(46) Tsai, M.-L.; Su, S.-H.; Chang, J.-K.; Tsai, D.-S.; Chen, C.-H.; Wu, C.-I.; Li, L.-J.; Chen, L.-J.; He, J.-H. Monolayer MoS_2 heterojunction solar cells. *ACS Nano* **2014**, *8*, 8317−8322.

(47) Baonza, V. G.; Taravillo, M.; Cáceres, M.; Núñez, J. Universal features of the equation of state of solids from a pseudospinodal hypothesis. *Phys. Rev. B* **1996**, *53*, No. 5252.

(48) Castro Neto, A. H.; Guinea, F.; Peres, N. M.; Novoselov, K. S.; Geim, A. K. The electronic properties of graphene. *Rev. Mod. Phys.* **2009**, *81*, No. 109.

(49) Giovannetti, G.; Khomyakov, P. A.; Brocks, G.; Kelly, P. J.; Van Den Brink, J. Substrate-induced band gap in graphene on hexagonal boron nitride: Ab initio density functional calculations. *Phys. Rev. B* **2007**, *76*, No. 073103.

(50) Tang, W.; Sanville, E.; Henkelman, G. A grid-based Bader analysis algorithm without lattice bias. *J. Phys.: Condens. Matter* **2009**, *21*, No. 084204.

(51) Gou, J.; Fan, B.; Song, G.; Khan, A. Study of affinities between the single-walled nanotube and epoxy resin using molecular dynamics simulation. *Int. J. Nanosci.* **2006**, *05*, 131−144.

(52) Ahangari, M. G.; Fereidoon, A.; Jahanshahi, M.; Ganji, M. Electronic and mechanical properties of single-walled carbon nanotubes interacting with epoxy: A DFT study. *Physica E* **2013**, *48*, 148−156.

(53) Grabowski, S. J.; Sokalski, W. A.; Dyguda, E.; Leszczyński, J. Quantitative classification of covalent and noncovalent H-bonds. *J. Phys. Chem. B* **2006**, *110*, 6444−6446.

(54) Baonza, V. G.; Caceres, M.; Nunez, J. Universal compressibility behavior of dense phases. *Phys. Rev. B* **1995**, *51*, No. 28.

(55) Brosh, E.; Makov, G.; Shneck, R. Z. The spinodal constraint on the equation of state of expanded fluids. *J. Phys.: Condens. Matter* **2003**, *15*, 2991.